

$\pi^-$ -BEAM STUDIES USING TIME-OF-FLIGHT METHODS

H. Appel, V. Böhmer, G. Büche, W. Kluge and H. Matthäy

Institut für Experimentelle Kernphysik der Universität und des Kernforschungszentrums Karlsruhe, Germany.

Abstract

Physical properties of the SIN pion beam  $\pi E3$  have been measured using time-of-flight techniques. In particular the momentum and the momentum band width were determined with an accuracy of  $\pm 0.5$  MeV/c and  $\pm 0.1$  MeV/c, respectively. The beam contamination with  $e^-$  and  $\mu^-$  as well as their local distributions have been measured under various conditions.

1. Introduction

The application of negative pions in cancer therapy and radiobiological research requires a detailed knowledge of the physical properties of the beams to be used.

The present paper deals with the results of beamdiagnostic measurements having been carried out at the biomedical channel  $\pi E3$  of the SIN accelerator. In particular the following parameters have been measured:

- a) the absolute beam momentum in dependence on different magnet settings;
- b) the momentum band width as a function of the momentum defining slit width for special magnet settings;
- c) the fractions of electrons and muons relative to the pion intensity as a function of the absolute momentum and the slit width for a beryllium and a molybdenum production target;
- d) the beam profile and the differential local distribution of the three beam components within different planes perpendicular to the beam axis.

2. Experimental technique

The SIN accelerator is an isochronous machine and therefore produces bursts which are short in comparison to the time interval of 20 nsec between subsequent beam pulses (corresponding to the RF of 50 MHz). This time microstructure is conserved even in the secondary  $\pi^-$ -beam. Together with a flight path of about 11 m due to the layout of the channel it favours the application of a special time-of-flight technique (TOF) for the measurement of the beam parameters listed above. The detailed description of this method can be found in ref.<sup>1</sup>). It is a particular feature of this method that the start signal is derived from the RF of the

cyclotron whereas the stop signal is taken from a detector. Another significant property of the TOF circuitry used throughout these experiments is the small differential non-linearity over the whole range of operation.

3. Results

3.1 Time-of-flight spectra

A typical TOF spectrum measured for a beam momentum setting of 150 MeV/c is shown in fig. 1. The three peaks corresponding to electrons, muons and pions are seen to be clearly separated.

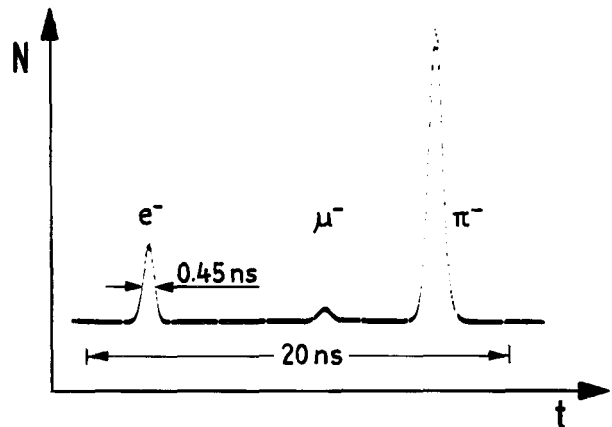


Fig. 1 Time-of-flight spectrum of the beam components  $e^-$ ,  $\mu^-$ ,  $\pi^-$  for a momentum setting of 150 MeV/c and a flight path of 10.92 m

It is obvious that from such spectra the relative fraction of the beam components can be determined with high accuracy as will be discussed in section 3.3. The width of the electron peak was evaluated to 0.45 nsec (FWHM). This overall time resolution includes the electronic resolution and a contribution from the time jitter due to the small but finite burst width.

Time-of-flight measurements of this kind can be combined advantageously with a measurement of the differential energy loss  $dE/dx$  of the particles. This provides the possibility to separate the pions from those muons originating from pion decay between the last bending magnet and the detector plane, both types of particles having almost the same TOF but different  $dE/dx$ .

The result of a combined  $dE/dx$  and TOF measurement is shown in fig. 2a as an isometric display. Fig. 2b presents a set of onedimensional time-of-flight spectra of the same type as in fig. 1. They were recorded for different magnet settings between 150 and 185 MeV/c in steps of 5 MeV/c in order to determine the absolute beam momentum and the dependence of the electron and muon contamination on the momentum. The same set of spectra is shown once more in fig. 2c as a map display, the brightness reflecting the number of counts per channel. This latter projection

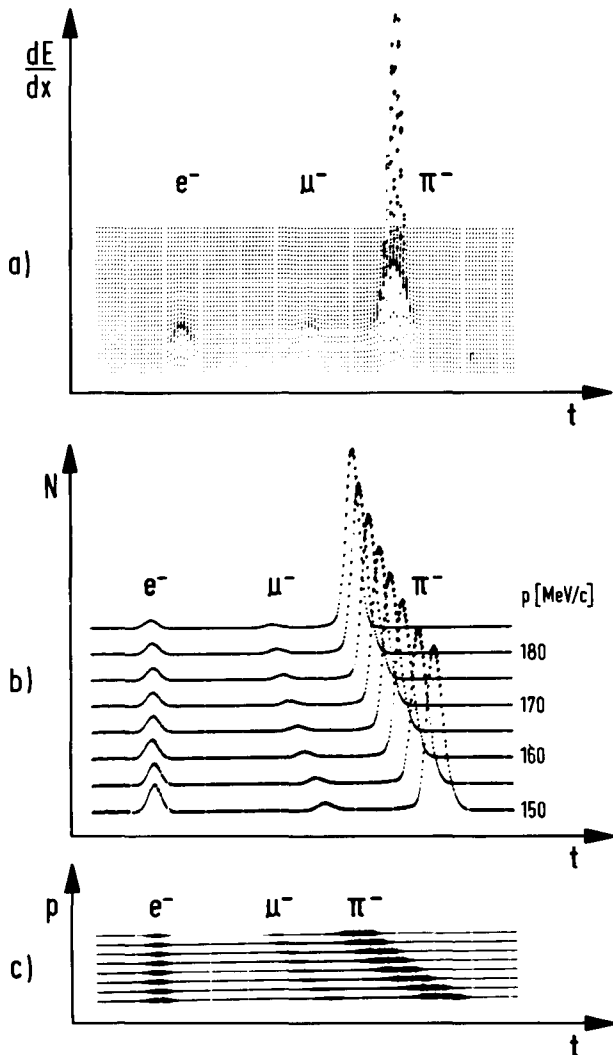


Fig. 2 a) Twodimensional  $dE/dx$  and TOF spectrum for a momentum of 165 MeV/c  
 b) TOF spectra for different momentum settings in steps of 5 MeV/c  
 c) The same spectra as shown in fig. 2b presented in a map display

demonstrates vividly the kinematical relation between time-of-flight and momentum. For pions and muons this relation is represented by a hyperbola whereas the TOF of the ultrarelativistic electrons is independent on their momentum.

Throughout the measurements discussed so far the width of the momentum defining slit FS 72 has been kept constant. In a separate set of measurements the band width of the momentum was varied with the centre momentum being kept fixed. Fig. 3 shows TOF spectra for a centre momentum of 150 MeV/c and four different slit widths.

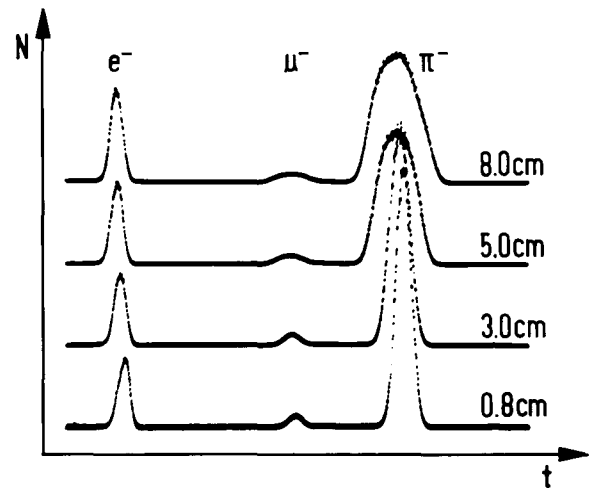


Fig. 3 TOF spectra for four different slit widths and a fixed centre momentum setting of 150 MeV/c

As a consequence of the increasing momentum spread the peaks due to pions and muons undergo a considerable broadening with increasing slit width whereas the electron peak is not affected at all.

### 3.2 Momentum and momentum band width

Taking into account the shape of the peaks in detail the careful analysis of the spectra shown in fig. 2b and c allows the determination of the absolute momentum of the beam with an accuracy of  $\pm 0.5$  MeV/c.

The true width of the momentum band as a function of the slit width has been evaluated from the broadened pion peaks of the spectra in fig. 3. Eliminating the experimental resolution numerically, the accuracy of the momentum band width obtained is  $\pm 0.1$  MeV/c. The results for a centre momentum of 175 MeV/c are shown in fig. 4.

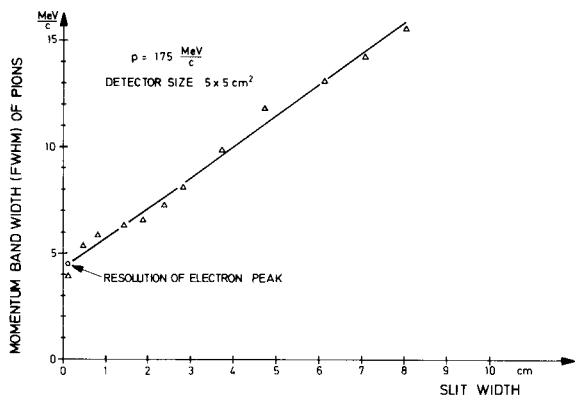


Fig. 4 The width of the momentum band as a function of the slit width for a fixed centre momentum of 175 MeV/c

### 3.3. Beam components

The contamination of pion beams with electrons and muons is expected to depend on various parameters. Therefore the components of the  $\pi E3$  beam produced from a beryllium target have been determined as a function of

- the momentum
- the momentum band
- the channel tuning
- the detector size and position.

One additional measurement was carried out with a molybdenum target<sup>2</sup>). Some results are shown in fig. 5.

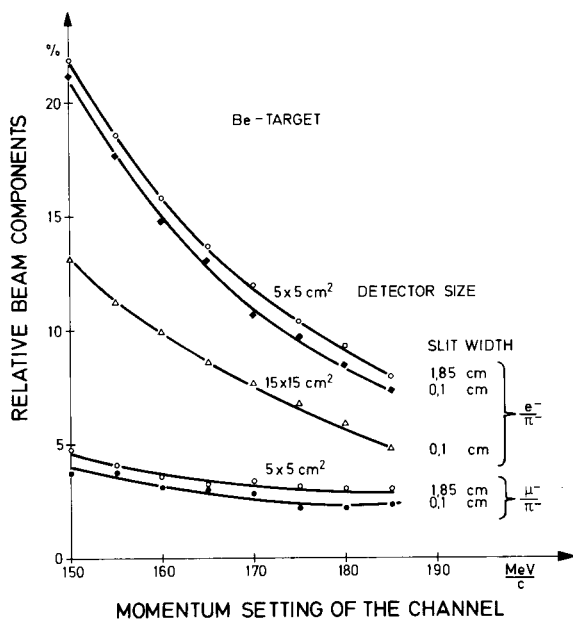


Fig. 5 The intensity ratios  $e^-/\pi^-$  and  $\mu^-/\pi^-$  as a function of momentum, slit width and detector size

The curves drawn in this figure indicate that the electron contamination decreases noticeably with increasing momentum. In the case of a beryllium production target, for a slit width of 0.1 cm and a detector size of  $15 \times 15 \text{ cm}^2$  the ratio  $e^-/\pi^-$  of the intensities of electrons and pions in the focal plane varies between 13% and 5% from momenta between 150 and 185 MeV/c, respectively. With a considerably smaller detector ( $5 \times 5 \text{ cm}^2$ ) a larger relative electron contribution varying between 21% and 7% was observed. This finding was thought to be of geometrical origin. Therefore measurements were started using a multiwire chamber. First results on this subject are reported in section 4.

On the other hand the  $\mu^-/\pi^-$  ratio remains almost constant over the whole momentum range. Further it turns out that neither the  $e^-/\pi^-$  nor the  $\mu^-/\pi^-$  ratio vary considerably with the slit width. The last result is demonstrated in more detail by fig. 6 for a momentum of 175 MeV/c and a detector of  $5 \times 5 \text{ cm}^2$ .

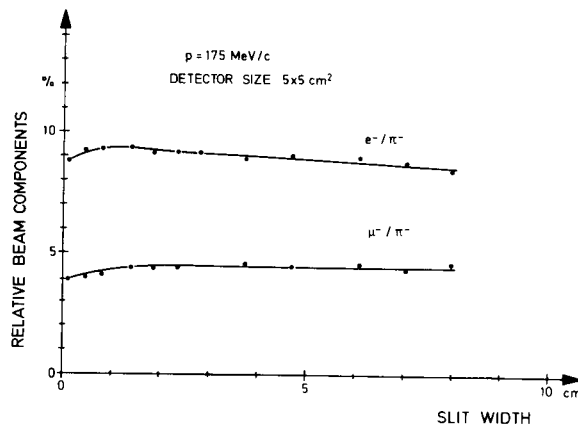


Fig. 6 The  $e^-/\pi^-$  and  $\mu^-/\pi^-$  ratios as a function of the slit width for a fixed centre momentum of 175 MeV/c

### 4. Beam spot measurements

In order to study the dependence of the beam components on the detector size the local distribution of each component was measured separately within the focal plane by means of a multiwire chamber of the hybrid type. This chamber combines the advantage of a simple magnetostrictive readout with a rather good time resolution of about 80 nsec. A detailed description of its principle of operation and its main properties can be found in ref.<sup>3</sup>). The chamber was triggered by a coincidence of two detectors of  $12 \times 12 \text{ cm}^2$  active area, placed above and below.

Figs. 7a to c show the local distributions of electrons, muons and pions within the focal plane for a special beam tuning. Fig. 7d demonstrates the broadening of the pion spot after insertion of 12 cm of carbon into the beam at a distance of 24 cm from the chamber.

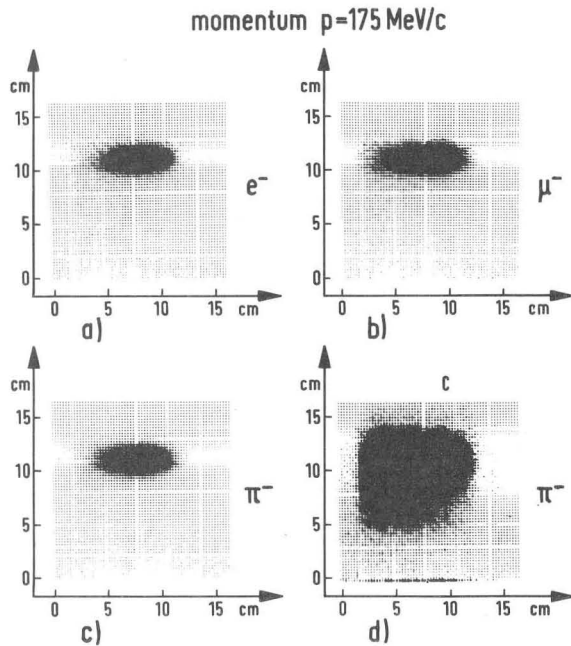


Fig. 7 Local distributions of electrons (a), muons (b) and pions (c) within the focal plane for a special tuning of the beam. In part (d) the pion distribution is shown after insertion of 12 cm of carbon.

The onedimensional projection of the different contributions to the beam spot onto the abscissae of fig. 7 reveal an increasing broadening for pions and muons relative to the electron distribution. The projection onto the ordinates, however, do not show any mutual differences in shape. Obviously the different local distributions of the beam components lead to a dependence of the intensity ratios  $e^-/\pi^-$  and  $\mu^-/\pi^-$  on the detector size which was mentioned in section 3. This influence of the detector geometry will be worked out in more detail.

#### References

- 1) H. Brückmann, E.L. Haase, W. Kluge, L. Schänzler, NIM 67 (1969) 29
- 2) H. Appel, V. Böhmer, G. Büche, W. Kluge, H. Matthäy, SIN Newsletter No.5(1975)26
- 3) V. Böhmer, NIM 107 (1973) 157